Cross-Front Mixing and Frontal Upwelling in a Controlled Quasi-Permanent Density Front in the Gulf of St. Lawrence

C. L. TANG

Bedford Institute of Oceanography, Dartmouth, N.S., Canada

(Manuscript received 28 June 1982, in final form 18 February 1983)

ABSTRACT

CTD data obtained from three transects across a controlled quasi-permanent density front in the Gulf of St. Lawrence were analyzed for the purpose of investigating cross-front mixing, mechanisms for frontal convergence, secondary circulation induced by the front and relationship between surface mixed-layer properties and frontal structure. Water mass analysis indicates that mixing takes place mainly in the ambient water, from the lower boundary of the frontal layer down to ~100 m. On the side of heavier water, there is a region of low surface temperature. The water masses have a distribution suggestive of upwelling in the low surface temperature region. The thickness of the surface mixed layer varies across the front. Outside the frontal zone there is a well-developed mixed layer of a thickness of about 25 m. It disappears completely in the low surface temperature zone and is re-established in the frontal layer with a reduced thickness. Horizontal intrusions below the frontal layer and interleaving of thin layers in the intermediate cold layer (40–100 m) were observed. A cross-front circulation is proposed to explain the observations. Two mechanisms to generate the cross-front flow and upwelling, i.e. the centripetal acceleration of water parcels flowing along a curved density surface and suction of subsurface water by an internal Ekman flow beneath the frontal layer, are discussed.

1. Introduction

Oceanic fronts participate in the cascade of energy and enstrophy from large to small scales. Their role in oceanic mixing, particularly in the boundary regions of water masses, has been recognized by many authors (Joyce, 1977; Needler, 1978; Garrett, 1979). Through observations and theoretical studies, many advances have been made in our understanding of the frontal characteristics and dynamics in the past decade (e.g., Mooers et al., 1976; Joyce *et al.*, 1978; Csanady, 1971; MacVean and Woods, 1980; Garvine, 1980; Kao, 1980). However, because of the complexity of the dynamics and the difficulty of making effective measurements, many frontal processes are still not fully understood. Some problems in frontal studies that need further attention have been identified by Mooers (1978) and Bowman (1977). The purpose of this paper is to attempt to answer some of the questions raised by these authors by a detailed analysis of field data.

The problem we are most concerned with here is the associated processes induced by a class of fronts characterized by sharp frontal interface, stationarity in position and strong along-front flow. The questions addressed in this paper are: How is the water mixed in the frontal region? Can such a front induce a secondary cross-front flow? What is the mechanism of frontal convergence that can keep the front sharp? Is there a change in the properties of the surface mixed layer across the front; if so, can the change be linked to the cross-front motion? It is obvious that the answers to these questions cannot in general be extrapolated to fronts with properties and generation mechanisms different from the one we consider here. To define the objectives of this study clearly, we emphasize the following:

1) The position and shape of the front and the frontal layer under consideration are controlled by some external factors, i.e., inflow of buoyancy and geometry of the coastline. Weak associated processes such as cross-front flow can be induced by the strong along-front flow, but the associated processes themselves are too weak to influence the first-order motions significantly. This situation is very different from a weak, broad and uncontrolled (or weakly controlled) front in which internal dynamics play an important if not a greater role than the external controlling factors such as wind, tides, topography and large-scale current system in determining the position and shape of the front.

2) The front under consideration is a relatively stable density front. The frontal layer is separated from the ambient water by a sharp interface. The most interesting structure in the temperature-salinity field is exhibited in the ambient water. Therefore, the focus of our analysis is the ambient water rather than the frontal layer itself.

The front we shall examine is situated in the northwestern corner of the Gulf of St. Lawrence (GSL) (see Fig. 1), a region of strong interactions between

the outflow of the St. Lawrence estuary and the GSL water. The most prominent oceanographic feature in this region is a coastal jet known as the Gaspé Current flowing seaward along the coast of the Gaspé Peninsula (the southern coast in Figs. 1 and 2). It is a relatively stable coastal current with a mean surface speed of 90 cm s^{-1} during the summer months, reducing to 60 cm s^{-1} toward November. In winter, it either becomes very weak or totally disappears (Benoit, 1980; El-Sabh, 1976). The water of the Gaspé Current comes from the upper 25 m of the St. Lawrence estuary; it is distinctly different from the water outside the Current. The boundary of the Gaspé Current defines a front which runs parallel to the coast. This front can be traced upstream along the coast and across the channel to reach Pointe des Monts on the north shore, as shown on the surface salinity map of Fig. 1. This frontal system is formed by the low salinity estuarine water encountering more saline and denser water of the GSL. The density difference of the two water masses creates a horizontal density gradient that drives an anti-cyclonic along-front geostrophic flow around the mouth. This flow carries the estuarine water downstream to form the Gaspé Current.

The frontal system can easily be identified in satellite imagery as a continuous band of cold surface water lying along the front (Tang 1980a). Its position does not change much throughout the summer except during occasional outbursts of violent events (Tang 1980b). The sampling strategy for the observations was designed in such a way that the low frequency motion and the tides would not cause distortions in the measurements severe enough to invalidate our interpretation of the data.

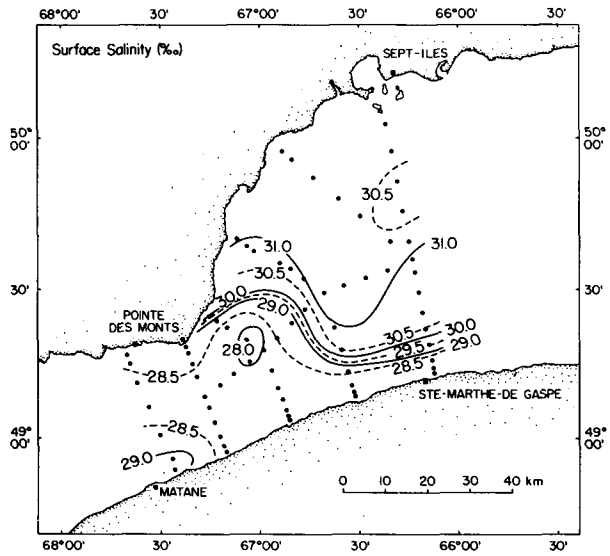

FIG. 1. Surface salinity of the northwestern Gulf of St. Lawrence (after Tang, 1980a) based on CTD data of 1978.

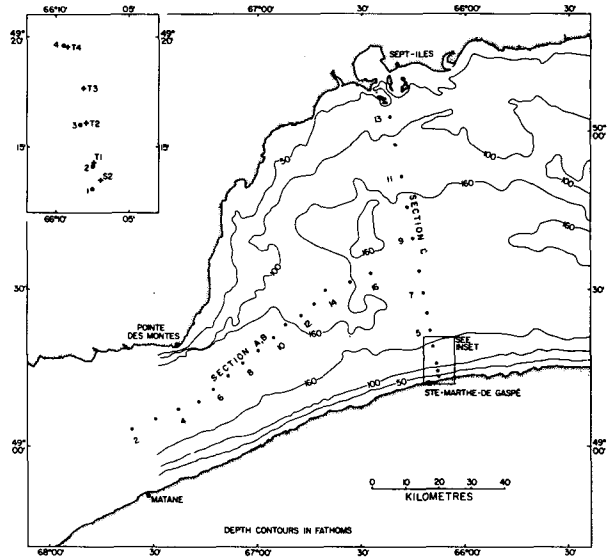

FIG. 2. Locations of CTD stations (solid circles) and current meter stations (crosses in the inset). Sections A and B have identical stations but are separated in time by 25 h.

2. Data

Data analyzed in this paper were collected during two cruises in 1978 and 1979 (Tang and Bennett, 1981; Tang, 1980a). The 1978 data set consists of 70 CTD stations covering the entire northwestern GSL (solid dots in Fig. 1), and three months of current-meter data from nine moorings near the south shore in the core of the Gaspé Current. A subset of the 1978 data will be used in this study (Section C in Fig. 2). We note that the east–west cross-front section will not be used because the stations in that section were not occupied consecutively. In the 1979 cruise, CTD data were obtained from two transects of the east–west section. Identical sets of stations were occupied during the two transects, but the times of the measurements were offset by 25 h. This time interval was chosen so that the two sets of measurements would represent the oceanographic conditions at the same phase of the tidal cycle. The two transects are designated as Sections A and B; the locations of the stations are shown in Fig. 2. Table 1 gives a summary of the data.

The hydrographic data were obtained with a Guildline Mark III CTD probe. For the study of small-scale features, the original data were used (obvious spikes and flat spots removed and time-constant corrections made). For the analysis of large-scale properties, such as water mass analysis and geostrophic-current calculations, the smoothed and interpolated data were used. The currents were measured with Aanderaa RCM-5 current meters with a sampling period of 20 min. The data were low-pass filtered and decimated to four points per day.

TABLE 1. Summary of data used in this paper.

Year	Type of measurement	Designation of sections stations, and depth of current meters	Start time and duration of measurement
1978	CTD	Section C Stations C1–C13	0440 GMT 23 Sep 11 h 4 min
	Current meter	Stations	June 17
		T2 14 m	98 days
		T2 56 m	98 days
		T2 94 m	98 days
		T2 146 m	98 days
		T3 20 m	97 days
		T3 150 m	97 days
		T4 12 m	97 days
		T4 144 m	97 days
1979	CTD	Section A Stations A2–A16	0116 GMT 29 Sep 8 h 42 min
		Section B Stations B4–B16	0309 GMT 30 Sep 7 h 37 min

3. Cross-front temperature-salinity structure

Figures 3–5 show the temperature, salinity, and density distributions on Sections C, A, and B (see Fig. 2). In the temperature–salinity range of the region, the density is mainly a function of salinity. Therefore, the density and the salinity sections are very similar.

Section C runs through the central part of the northwestern GSL, where the circulation is dominated by a basin-wide permanent cyclonic gyre. The sloping isopycnals below 60 m near the shore reflect the general direction of the mean currents, westward in the north and eastward in the south. In the middle part of the section (C6 to C11) there is a well developed surface mixed layer. It gradually disappears toward the north shore, possibly as a result of increased tidal mixing as the water becomes shallower (Pingree and Griffiths, 1980). Near the south shore the structure is more complex. Superimposed on the dome-like background is the Gaspé Current, which has a surface salinity 2‰ lower than the surrounding water. The temperature variation across the Gaspé Current is interesting. At the edge of the current there is a minimum in surface temperature (Station C4). Below the surface, a slight rise in the isotherms and isohalines can be seen.

Sections A and B represent the cross-front sections without a coastal wall on either end. Absence of the coast eliminates the coast-induced processes, such as tidal mixing. The two sections show much similarity. The frontal layer can clearly be identified in the salinity and density sections. The outcrop of the isohalines and isopycnals occurs mainly between Stations 8 and 9 (for Section A) and Stations 10 and 11 (for Section B). In the ambient water, the isopycnals and isohalines are somewhat depressed below the frontal layer and raised outside the frontal layer. The temperature sections have more structure and are different from the salinity and density sections in that the frontal layer can no longer be identified. The surface temperature of the frontal layer is the same as that in the extreme east of the section (Stations 14 to 16). On the other hand, an area of low surface temperature is in between Stations 11 and 12. This is in agreement with the band of cold surface water along the front seen in the satellite imagery (Tang, 1980a). Like Section C, a well-developed surface mixed layer exists far away from the front. The fact that the surface mixed layer does not extend to the tip of the frontal layer suggests that mixing and vertical motion are probably strong in the transition zone and can hinder the development of a surface mixed layer.

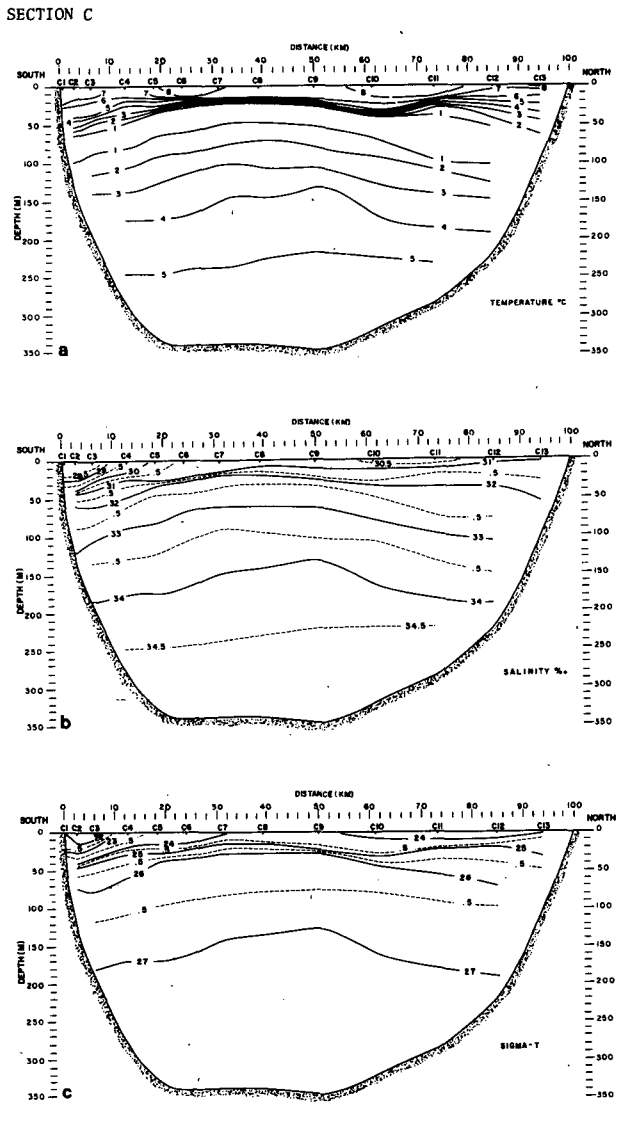

FIG. 3. (a) Temperature, (b) salinity and (c) σ_t of Section C.

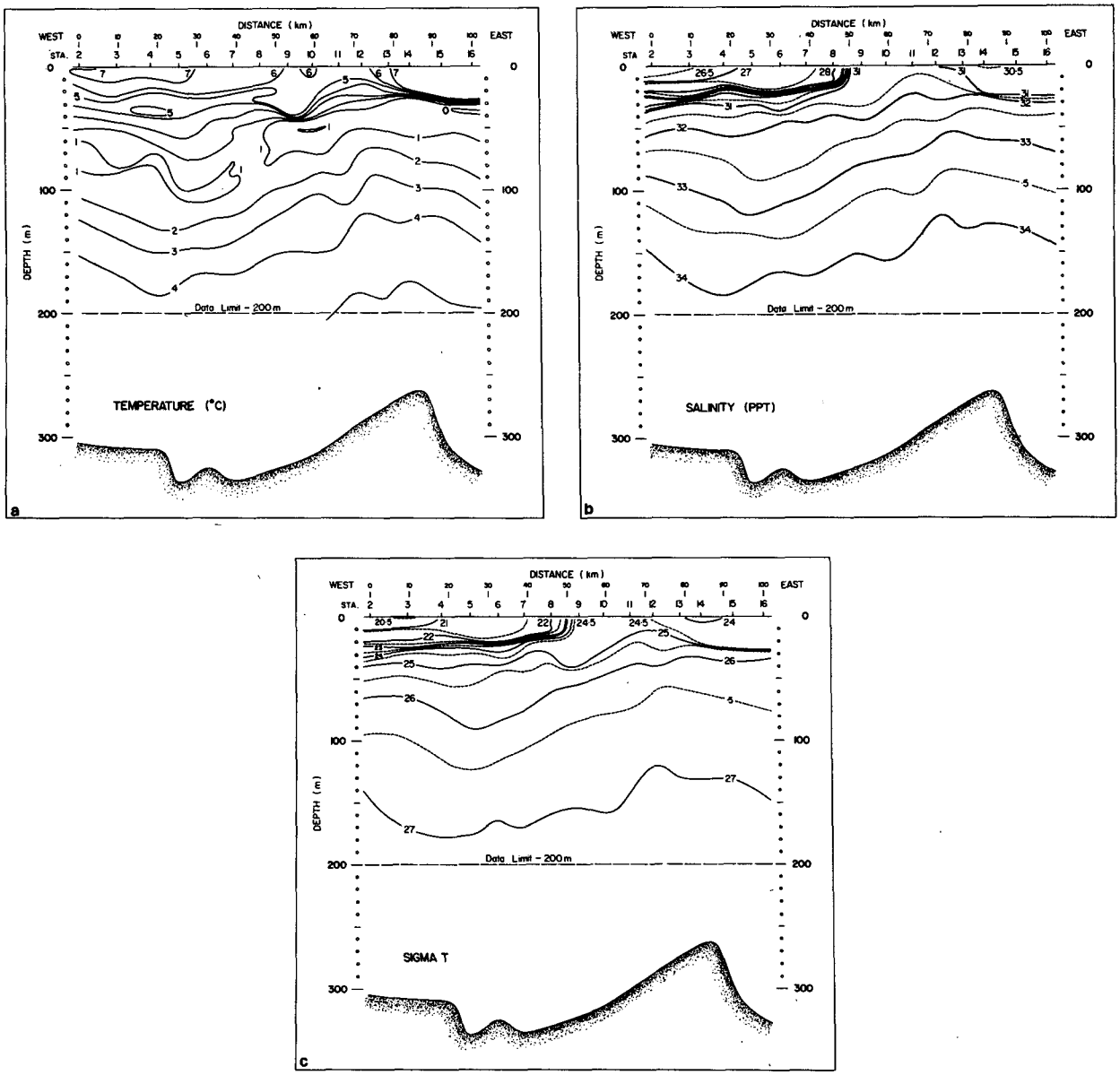

FIG. 4. (a) Temperature, (b) salinity, and (c) σ_t of Section A.

A comparison of Sections A and B reveals that the tip of the frontal layer has moved eastward ~15 km in 25 h (16 cm s^{-1}). However, if we consider the 28‰ isohaline as the boundary enclosing the bulk of the low salinity water of the frontal layer, then both the position and the shape of the frontal layer appear little changed from A to B. The thinning of the frontal layer from B9 to B11 suggests that perhaps only the water near the tip spread to B11, while the rest of the frontal layer remained stationary.

In all three sections, a layer of cold water exists between 40 and 100 m. In Sections A and B the temperature in this cold layer varies across the sections, being colder outside the frontal zone and slightly warmer near the estuary. The difference in the minimum temperature across the front is approximately 1°C. Within this broad-scale variation, regions of slightly warmer water exist below the frontal layer, centered around A8 at 70 m and B11 at 60 m. This suggests an enhanced vertical mixing in localized regions of the frontal zone.

4. Water masses

The T–S diagrams for selected stations across the front are shown in Fig. 6; C7 and A15 are representative of the stations outside the frontal zone, which are characterized by a well developed surface mixed

layer (see Fig. 12) and a classical T–S relationship from vertical mixing of three water types. The three water types are:

1) *The Gulf surface water.* This water type has a temperature of 7–8°C and salinity ~30.8‰. It exists throughout the entire GSL and changes gradually from one part of the GSL to another, but the spatial scale of the change is much larger than that in the frontal zone.

2) *The intermediate cold water.* The existence of a cold layer at the intermediate depths of 60 to 80 m has been recognized since the early 1940's when modern oceanographic surveys in GSL began. The cold layer is believed to form locally during winter and is distributed over the entire St. Lawrence system including the estuary. The temperature of the layer has an annual cycle, decreasing from a maximum value of 1°C in the winter to a minimum of −1°C in May (Ingram, 1979).

3) *The deep water.* Below the intermediate cold layer the T–S values fall on a universal line indicating the common origin of the deep water. It exists in every part of the GSL with a depth greater than 100 m and has an almost constant salinity of 34.6‰ and temperature of 4.7°C (Forrester, 1964).

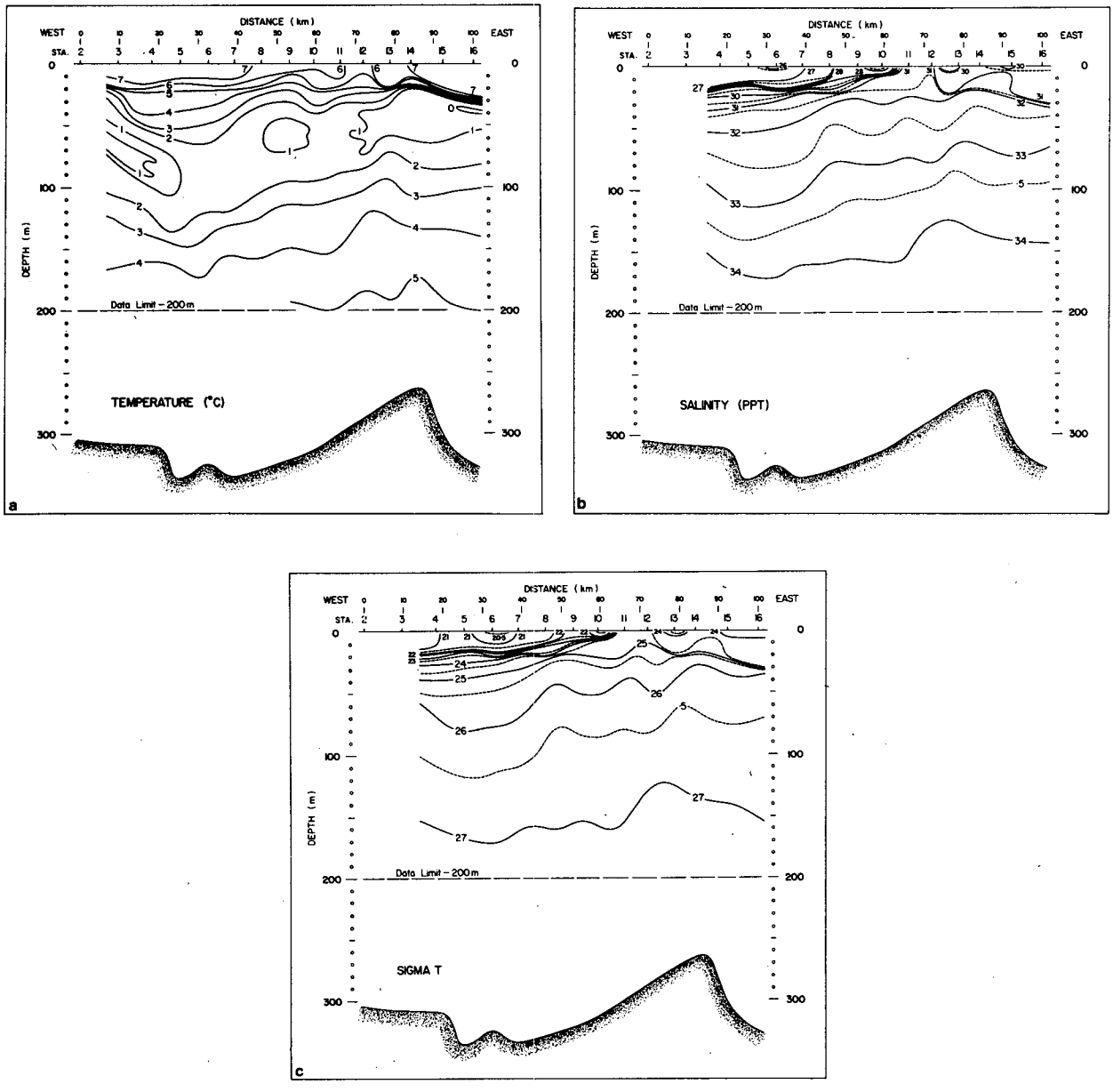

FIG. 5. (a) Temperature, (b) salinity and (c) σ_t of Section B.

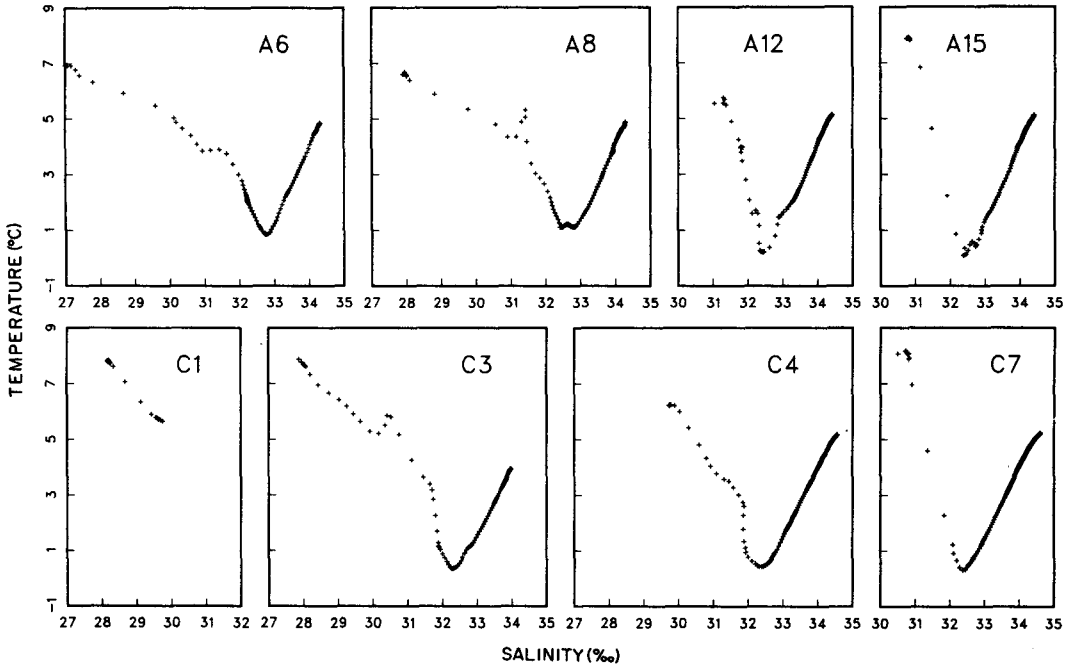

FIG. 6. *T–S* diagrams for selected stations. The data were smoothed and interpolated every 2 db.

At the surface of the frontal layer (Fig. 6), a fourth water type is present (A6 and C1).

4) *The estuarine water.* This water type is considerably fresher than the other three types with a salinity of 27‰ at A6 and 28.15‰ at C1. Inside the estuary, it mixes directly with the intermediate cold water. In the frontal zone it further mixes with the mixture of *a* and *b* as can be seen in the *T–S* diagrams of A6, A8, and C3 (Fig. 6).

A close examination of the *T–S* diagrams across the front reveals some interesting facts. Stations A12 and A15 have the same *T–S* relationship but the surface temperature of A12 is lower than that of A15 by 2.5°C. A comparison of the vertical profiles (Fig. 11) shows that below 60 m the water column of A12 is raised ~10 m over that of A15. Above 60 m the *T–S* profiles of the two stations are quite different. The vertical structure will be further discussed in Section 6. The station in Section C with the lowest surface temperature is C4. The difference in the *T–S* relationship between C4 and A12 is that the upper water column of C4 has a high content of estuarine water, which is not found in A12. The absence of a station in Section C with a *T–S* curve resembling that of A12 may be due to insufficient horizontal sampling.

The *T–S* relationships can be summarized by the diagram in Fig. 7. Outside the front, the water mixes vertically and follows the curve *abc*. In the frontal layer the water is composed mainly of the estuarine water *d*. Below the frontal layer the estuarine water mixes with the mixture of *a* and *b*, denoted by *e* in Fig. 7, forming the curve *de*. From the depth corresponding to *e* to the bottom, the *T–S* characteristics are the same as the water outside the front, following the curve *ebc*.

Between the stations, characterized by a *T–S* relation of the type *abc* and those of the type *debc*, is a region of transition (A10 to A12, C4) in which the surface temperature is significantly lower than that of either of the two types. The *T–S* relation in this region is represented by a_1bc (A12) and d_1ebc (C4). The lower surface temperature can be a signature of upwelling or enhanced vertical mixing.

5. Percentage content of water masses

To determine the distribution of water masses in a vertical section, we use the classical method of mixing triangle to calculate the percentage compositions. From the *T–S* diagrams in Fig. 7, it is obvious that any point on and to the right of line *ab* is a mixture of *a*, *b*, and *c* without the involvement of the estuarine water. A point to the left of line *ab* can only be mixed from *d*, *a*, and *b*, since in the physical space *c* lies below *b*, and it is physically impossible for it to participate in the mixing. Using the triangles *cba* and *dba*, we calculated the percentage content of the three pure water types *d*, *c*, and *a*. The results are shown in the top two panels of Figs. 8, 9, and 10.

A similar calculation could be done for the intermediate cold water *b*, which lies around 100 m below the frontal layer, and around 40 m outside the front.

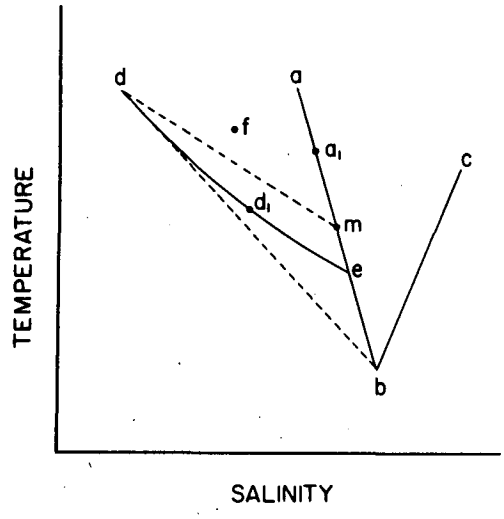

FIG. 7. Schematic diagram summarizing the T–S relationships shown in Fig. 6 where a is the Gulf surface water, b is the intermediate cold water, c is the deep water, and d is the estuarine water.

However, since the most interesting features in the T–S field occur between the surface and the intermediate cold layer, it is more informative to study the distribution of the water with T–S values between a and b. We define the "mixed water" as a water type composed of 50% of a and 50% of b (denoted by m in Fig. 7) and calculate the percentage content by subdividing dba into two smaller triangles dma and dmb. It should be noted that the meaning of the percentage content for a mixed water type is ambiguous. Thus the results for the mixed water m should be interpreted as the distribution of a parameter indicative of the closeness of a point to m in the T–S diagram. The results are shown in panel (c) of Figs. 8 to 10.

The estuarine water is present only within the frontal layer as expected. The deep water is smoothly distributed over the entire section. Below the intermediate cold layer, the T–S relationship is linear; hence the percentage content of deep water is basically a reflection of the temperature and salinity distributions. Most of the structures in the percentage content may appear in the Gulf surface water and the mixed water. The highest concentration of Gulf surface water is in the region farthest from the front in the upper 20 m. Anomalous concentrations are found below the frontal tip at 30 to 40 m in Section A and 25 to 35 m in Section C. The mixed water has S-shaped contours from Stations 8 to 13 in Section A and from Stations 3 to 5 in Section C. The dip in the contours of Gulf surface water and the mixed water around A5 and B5 below 50 m is much sharper than the gentle depression in the contours of the deep water, and is probably not simply a reflection of the large-scale circulation.

The gross features in the percentage content maps do not change appreciably from Sections A to B. However, because of the appearance of a double front in Section B, the features we identified in Section A are somewhat obscured by the presence of wiggles in the contour lines in Section B. It appears that as the tip of the frontal layer moves eastward, some features in the ambient water also shift eastward. The locations of the peak and trough of the S-shaped contour lines have moved from A11 and A9 to B13 and B10.

To determine the sensitivity of the results from the T–S values of the four pure water types, we have used a range of values corresponding to the scattering. The results differ very little from the ones we presented. The fluctuations in the T–S fields were calculated by Tang (1980a) using current meter data and repeated CTD casts over a semidiurnal tidal period at one-hour intervals for a station near the south shore of Section C. The rms temperature and salinity attributed to surface and internal tides are much smaller than the T–S variations associated with the features we have identified. Direct advection by the tidal cur-

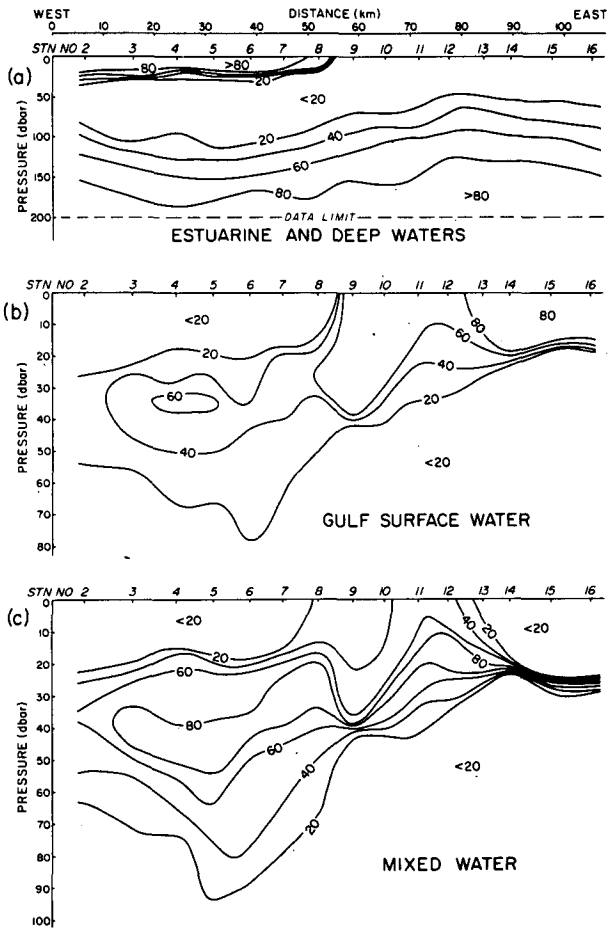

FIG. 8. Percentage contents of (a) the estuarine and deep water, (b) the Gulf surface water, and (c) the mixed water in Section A.

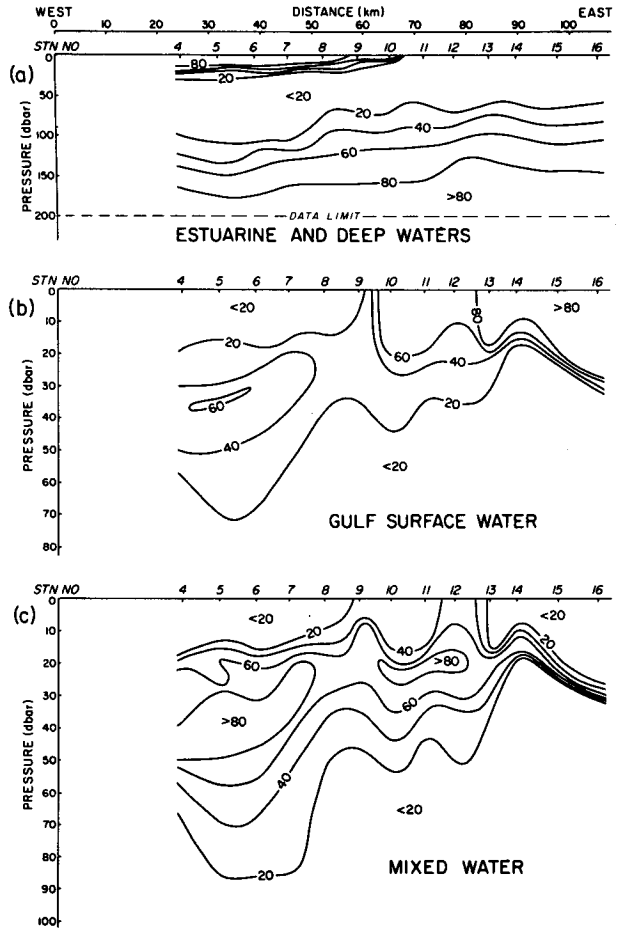

FIG. 9. As in Fig. 8 but for Section B.

rents cannot possibly cause the variations in T–S we observed since the horizontal scales of the features, 10–30 km, are much larger than the excursion distances of the tides, 1.4 km and 0.7 km at 20 m and 60 m, respectively. Possible contamination by internal waves can be checked by the extensive *Batfish* data taken in this area (Tang and Bennett, 1981). The fluctuations in vertical displacement of the isotherms and isopycnals indicated in the *Batfish* data are of the order of 15 m peak-to-trough. The structure shown in our data has a vertical length scale of typically 30 m or greater, and, more importantly, is position-locked (relative to the frontal layer). The presence of the internal waves is thus unlikely to distort the gross features we found in our data set.

Benoit (1980) analyzed three months of current meter records across the Gaspé Current; he found that the temperature at T3 around 20 m was persistently lower than for the neighboring current meters by ~2.5°C, which is consistent with our conclusion of a low-temperature zone associated with the front. In summary, we have some confidence that the structure revealed in the three sections is closely linked to the presence of the frontal layer, rather than coincidentally caused by some high-frequency motions. Perhaps the clearest surface manifestation of the correlation between the front and the T–S fields which defies any explanation by short-period variability is the persistent and continuous band of cold surface water along the front seen in satellite images.

6. Surface mixed layer

In order to study the small-scale structure (1 to 10 m) of the frontal region, the original data without smoothing and decimation but with time-constant corrections were examined. Figure 11 shows the temperature profiles of the upper 100 m from A4 to A15.

The mixed layer can clearly be identified from the vertical profiles by the homogeneity of the properties within the layer and the abrupt change at the base of the mixed layer. In Fig. 12, the thickness of the mixed layer is plotted against the cross-front distance for all three sections. At some stations (A14, C9, C2, C3), the mixed layer has a step-structure, which is denoted in the figure by two dots, the lower one cor-

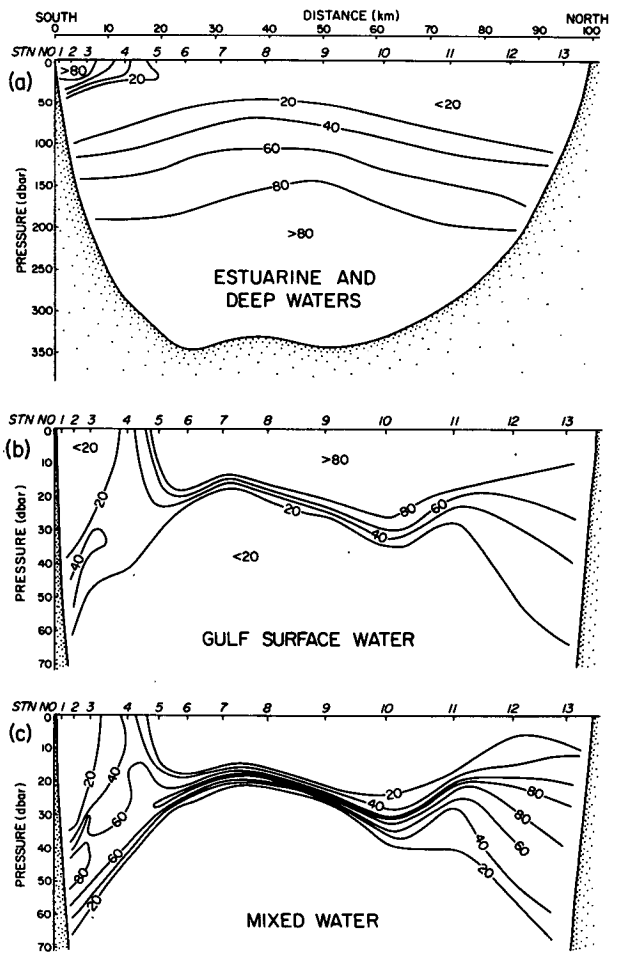

FIG. 10. As in Fig. 8 but for Section C.

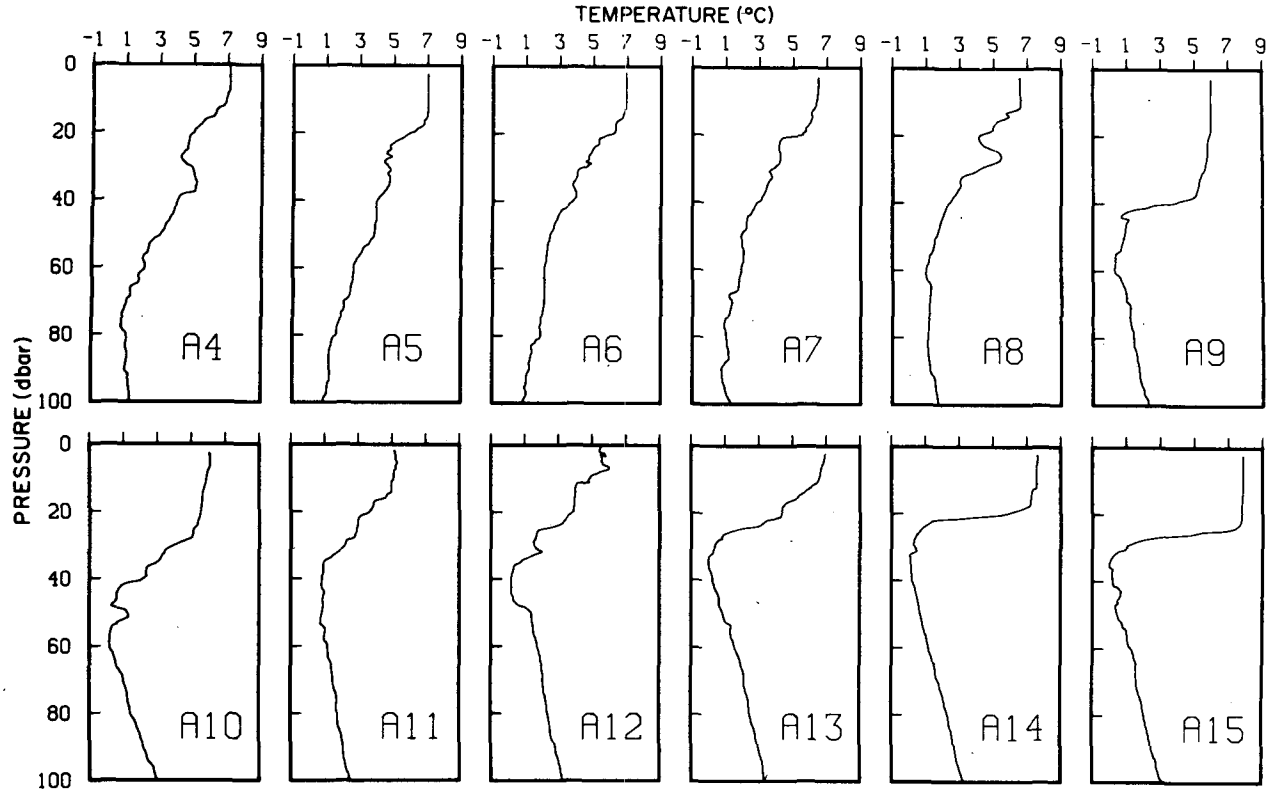

FIG. 11. Temperature profiles of A4 to A15 from 0 to 100 m.

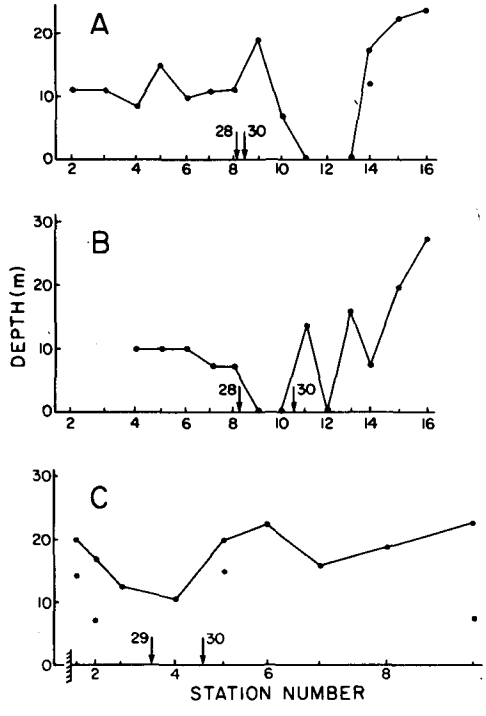

FIG. 12. Thickness of the surface mixed layer in Sections A, B, and C. The arrows indicate the positions of the outcrop of two isohalines. The numbers by the arrows give the salinity values of the isohalines.

responding to the depth of the step. The arrows indicate the position of the outcrop of two selected isohalines (28 and 30‰ for A and B, 29 and 30‰ for C). Their closeness in position is a crude measure of the sharpness of the front.

In Section A, the thickness of the mixed layer decreases from 24 m at A16 to 0 at A13. There is no identifiable mixed layer from A13 to A11. At A10 it reappears, and at A9 it becomes almost as thick as at A16. But the profile of A9 differs from that of A16 in that the base of the mixed layer does not coincide with (or is close to) the depth of rapid change in temperature. There is a thick transition zone from 18 to 40 m linking the two. This suggests a stretching of the water column below the mixed layer. Inside the front, from A8 to A2, the mixed layer is thinner than at A9 and does not undergo further drastic changes in thickness.

The frontal position in Section B is not so well-defined as that in A. But despite the ambiguity in the frontal position, the general features of the mixed layer are similar to those of Section A, such as maximum thickness in the extreme east, complete disappearance just outside the front, and reduced thickness inside the front.

The front at the edge of the Gaspé Current (Section C) is less sharp than that in Sections A and B. A mixed layer with varying thickness is present at all

the stations. There is no significant difference between the thickness at stations near the coast and those in the middle of the channel (C8 and C9). The station with the thinnest mixed layer is C4, which is also the station with the lowest surface temperature.

7. Horizontal intrusion

Interleaving in broad frontal zones with density-compensating T–S fields has been studied by many authors (Joyce *et al.*, 1978; Horne, 1978; Coachman and Charnell, 1979). The GSL front is a density front and thus interleaving is not expected to take place along the boundary of the frontal layer. A close examination of the vertical profiles, however, shows that isolated instances of folding of the isotherms and intrusions of thin layers take place in two regions: in the intermediate cold layer, as exemplified by the single intrusive layer at 50 m at A10, and below the frontal layer, as exemplified by the folding at 20 to 30 m at A8 (see Fig. 11). To investigate the nature of these features, we plotted the T–S diagrams using the unsmoothed data (Fig. 13). The intrusive filament at A10 is approximately aligned with the constant density lines. The intrusion is apparently caused by the presence of warmer water at A7 and A8 in the intermediate cold layer, which creates a temperature gradient along the isopycnals. A comparison of the T–S diagrams for A8 and A10 shows clearly that mixing cuts out the lowest part of the T–S curve of A8. This suggests an enhanced mixing in localized regions of the intermediate cold layer.

A natural vertical scale l for double-diffusive layers has been proposed by Ruddick and Turner (1979):

$$l = \alpha \Delta T \Big/ \left(\frac{1}{\rho} \frac{d\rho}{dz} \right),$$

where ρ is the density, ΔT the temperature difference between the two neighboring water masses along the isopycnals, and $\alpha = \rho^{-1} \partial \rho / \partial T$. Appropriate values of the parameters for A10 are $\Delta T = 1.2°C$, $\alpha = 0.6 \times 10^{-4}$ °C^{-1}, and $\rho^{-1}\, d\rho/dz = 14.2$ m^{-1}, from which we get $l = 5.5$ m. The thickness of the layer at A10 from the vertical profile is 5 m. The agreement in the order of magnitude between theory and observation indicates that the intrusive layer we observed is consistent with double-diffusive intrusion. Other stations which also show a layer-structure in the intermediate cold water are A13, A14, B12, and B8 (see Fig. 14).

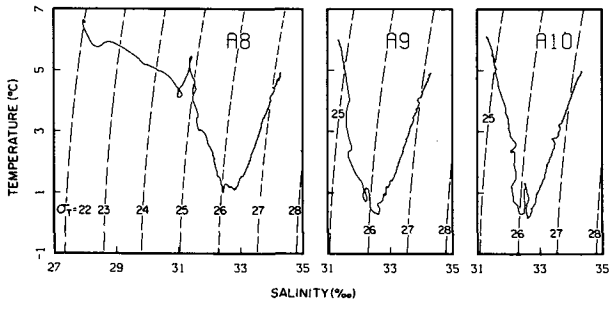

FIG. 13. T–S diagram for A8, A9, and A10 using the unsmoothed data.

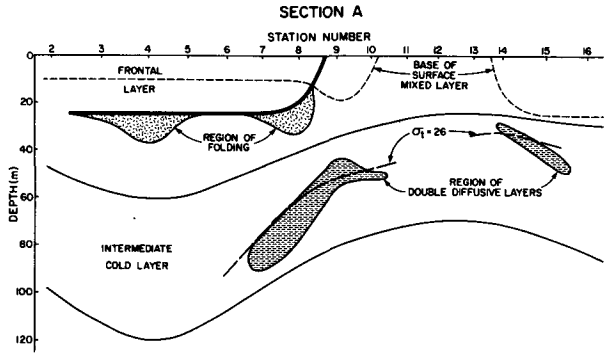

FIG. 14. Summary of small-scale features in Section A. The heavy solid line on the lhs of the figure denotes the lower boundary of the frontal layer. The two light wavy solid lines across the whole figure represent the 2°C isotherm which encloses the intermediate cold layer.

The folding of the isotherms at A8 from 20 to 30 m beneath the frontal layer has an entirely different origin from the intrusive layer just discussed. This is obvious from an inspection of the T–S diagram in Fig. 13 and the vertical temperature profile in Fig. 11. The warm layer has a thickness of 10 m, twice that of the double-diffusive layer in A10. The water in it is composed largely of Gulf surface water. The warm layer apparently results from the intrusion of Gulf surface water beneath the frontal layer. Since the environment for double-diffusive processes does not exist here, the intrusion we observe is probably caused by a cross-front flow. In addition to A8 folding of the isotherms in varying degrees is found at A3, A4, and A7. Fig. 14 summarizes the small-scale features in Section A that we have discussed in this section.

8. Scales and momentum balance of motion

The momentum balance of the frontal zone will be examined by comparing the geostrophic currents with the measured currents.

Figure 15 shows the geostrophic current for Section C calculated with the bottom as the level of no motion. The geostrophic current is strongest between C3 and C4. Strong shears are concentrated along the lower boundary of the frontal layer. The ambient water flows eastward in the south and westward in the north, in agreement with the previous observations of a permanent cyclonic gyre in the central part of the northwestern GSL (El-Sabh, 1976).

Current data were obtained from a mooring array across the Gaspé Current (see Fig. 2). To compare the measured currents with the geostrophic current,

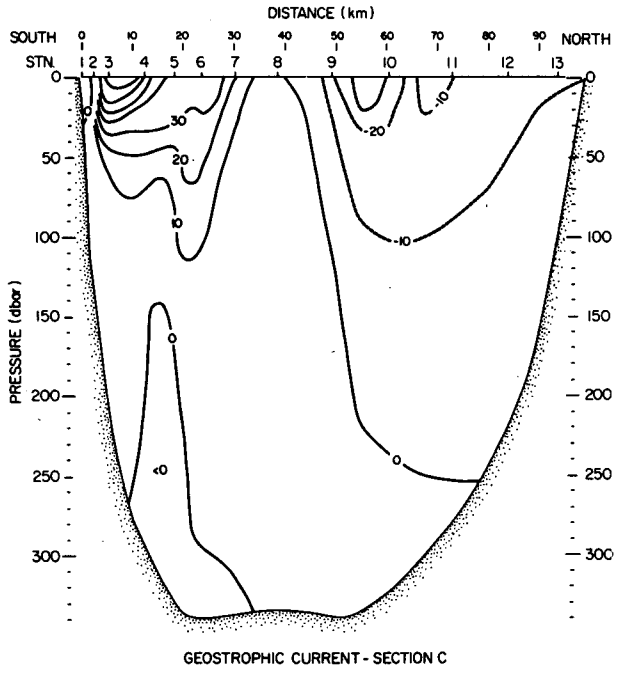

FIG. 15. Geostrophic current in cm s^{-1} for Section C. The level of no motion is taken at the bottom. Positive values (solid lines) indicate eastward currents, and negative values (dashed lines) indicate westward currents.

we use the mean current calculated from the last day of the current-meter records, which was one day before the CTD data were taken. Since the dominant variance of the subtidal fluctuations is in the 8- to 12-day band (Benoit, 1980), the one-day difference is not expected to introduce large errors in the comparison. Moorings T3 and T4 have current meters at two depths, and T2 at four depths; T1, S2, and the CTD station closest to the shore are not used, to avoid possible difficulty in interpretation. Figure 16a shows the mean current at T2, T3, and T4 normal to Section C3–C4 and the geostrophic current through the section. To make use of the better vertical resolution of T2, geostrophic currents through the station pairs (C2, C3) and (C3, C4) are linearly interpolated to the position of T2 horizontally, and to depths below the maximum depth of the (C2, C3) pair vertically. The interpolated geostrophic current and the current at the four depths of T2 are shown in Fig. 16b. In both Figs. 16a, b the geostrophic currents have been normalized at the depth of the deepest current meter. The agreement between geostrophic currents and the measured currents is reasonably good.

Geostrophic currents for Sections A and B are shown in Fig. 17. Similar to Section C, there are sharp current gradients across the front in Section A and an area of weak current at the intermediate depths just outside the front. The picture for Section B is less clear. Weak currents appear at B9, B10 and B12, and the core of the frontal current has split into two branches centered between B7 and B8 and between B10 and B11. Without current data from direct measurement, it is difficult to say with certainty whether the cross-front momentum balance is geostrophic. We can only rely on a scale analysis to estimate the main balance.

We have noted earlier that the change in the position of the front from Sections A to B probably involves only a small volume of water at the tip of the frontal layer, and the bulk of the frontal layer remains fixed in position. Under such circumstances, the front can be considered stationary. An alternative view is that the whole frontal layer has moved eastward by 12 km in a day (14 cm s^{-1}) from between A8 and A9 to between B10 and B11, which corresponds to a constant acceleration of 3×10^{-4} cm s^{-2}. This is an order of magnitude smaller than the Coriolis acceleration of 50×10^{-4} cm s^{-2} based on an along-front velocity (V) of 50 cm s^{-1}. Nonlinearity is measured by the Rossby numbers $U^2/(fLV)$ and $U/(fD)$, where L and D are the cross-front and along-front length scales, respectively. Using L = 40 km, D = 80 km (channel width), U = 20 cm s^{-1}, we get 0.02 and 0.025 for the two Rossby numbers. These order-of-magnitude calculations suggest that the cross-front momentum balance for Sections A and B is mainly geostrophic apart from a possible curvature effect as will be discussed in the next section. The small east–west motion of the frontal layer is not likely to change the dominant momentum balance.

Cross-front geostrophy is probably a universal feature in many types of oceanic fronts. Theoretical and

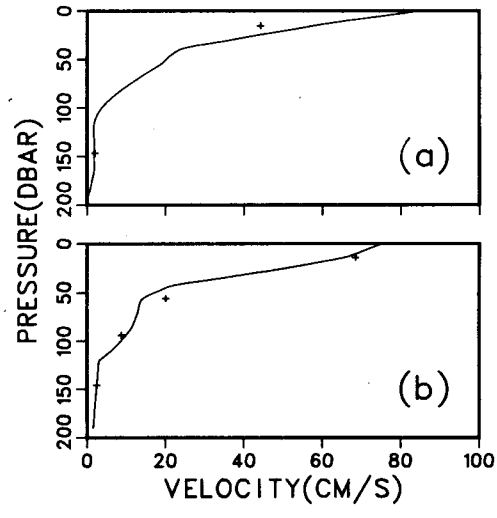

FIG. 16. Comparison of geostrophic current (solid lines) and measured current (crosses). (a) The geostrophic current was calculated from the station pair (C3, C4) and the measured current is the average of T2, T3, and T4. (b) The geostrophic current was calculated from the station pairs (C2, C3) and (C3, C4) linearly interpolated to the position of T2. The measured currents are from T2 at four depths. The geostrophic currents in both (a) and (b) have been normalized at the depth of the deepest current meter.

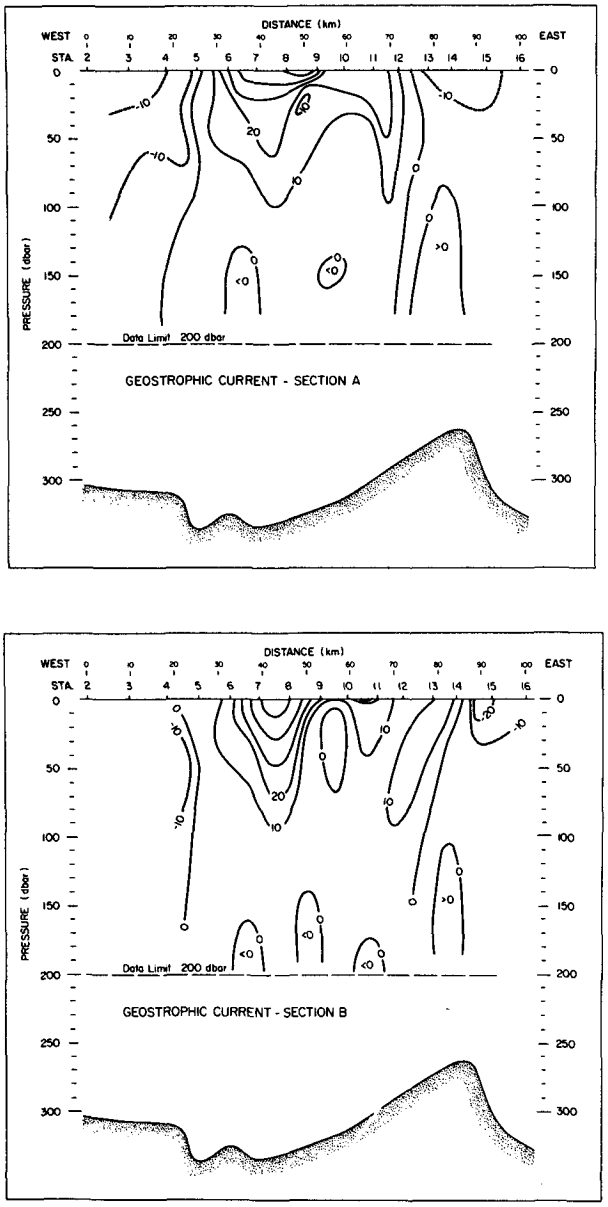

FIG. 17. Geostrophic current in cm s^{-1} for Sections A and B. The level of no motion is taken at the bottom. Positive values (solid lines) indicate southward currents, and negative values (dashed lines) indicate northward currents.

numerical studies of fronts (MacVean and Woods, 1980; Csanady, 1971; Hoskin and Bretherton, 1972) often employ cross-front geostrophy as a basic assumption of the models, giving consistent results with observations. Nonlinearity in frontal dynamics manifests itself mainly in the potential vorticity associated with the strong horizontal shear in the along-front direction, which is strongest near the tip of the frontal layer. Away from the frontal layer, the motion can be governed by dynamics quite different from the highly nonlinear dynamics of the frontal layer.

9. Discussion of cross-front flow and mixing

In the previous sections, we have seen features in the T–S fields associated with the GSL front. The main findings are:

1) The distribution of the water masses in the vertical sections shows an S-shaped pattern (Figs. 8–10) across the frontal zone.
2) The surface mixed layer near the front disappears or becomes thin in comparison to that far away from the front (Fig. 12).
3) Horizontal intrusion of the Gulf surface water occurs beneath the frontal layer (Fig. 14).
4) In the intermediate cold layer, the temperature around the frontal region is slightly higher than that outside the frontal region, and interleavings occur in the boundary region of the high temperature zone (Figs. 4, 5, 14).

In the absence of direct measurements of vertical motion and mixing, we shall postulate a cross-front circulation and examine whether our observations as summarized above are consistent with the assumption. We then investigate whether there are mechanisms which can produce such a cross-front circulation. The distribution of the water masses suggests a vertical motion with upwelling outside the front and downwelling below the frontal layer. A possible circulation pattern is shown in Fig. 18. Since Section A has the most clearly defined front, we shall use Section A for our discussion and the station numbers in Fig. 18 correspond to those of Section A. From Fig. 18, above 20 m the upward and downward velocities are greatest at A11 and A9, respectively. The vertical motion could give rise to an S-shape structure in the percentage-content contours of both the Gulf surface water and the mixed water. The upwelling could also result in a zone of low temperature from A10 to A12. The upwelled water flows westward to-

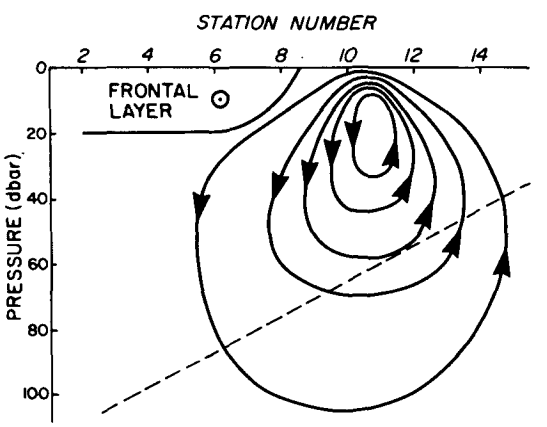

FIG. 18. Streamlines of the postulated cross-front circulation. Circulation below the dashed lines is less certain than that above.

wards the front before sliding under it. Such a horizontal flow could provide the necessary surface convergence that keeps the front sharp. The cross-front flow moving along and beneath the lower boundary of the frontal layer could cause an intrusion of the Gulf surface water at A8. Vertical motion in the intermediate cold layer could enhance mixing and give rise to a high-temperature zone, which could in turn trigger double-diffusive interleavings. The variation in the thickness of the mixed layer appears to be consistent with the proposed cross-front circulation. The thinning and disappearance of the mixed layer from A10 to A13 could be caused by an upward movement of the water column at a rate faster than the deepening rate by wind mixing.

Woods *et al.* (1977) noted that in a curved front the centripetal acceleration of a water parcel flowing along a curved constant-density surface could cause a vertical motion. The GSL front as defined by the surface salinity distribution of Fig. 1 has a curvature of about 10 km from Pointe des Monts to the mid-channel, and a similar curvature but of opposite sign from the mid-channel to the south shore. The curvature gives a centripetal acceleration of 2.5×10^{-3} cm s^{-2}, which is comparable to the Coriolis acceleration of 5×10^{-3} cm s^{-2}. Thus a water particle flowing horizontally along the curved density surface across the channel will experience an acceleration in a direction first upward and then downward. The upwelling seen in Sections A and B could be a manifestation of the upward acceleration. However, this mechanism cannot be responsible for the upwelling along the edge of the Gaspé Current (Section C), which flows along an almost straight coastline.

Another possible mechanism for frontal upwelling is the Ekman suction from a vertical-shear layer. Coastal upwelling is the most familiar example of this mechanism. In the ocean interior, a vertical-shear layer can exist if there is a discontinuity in the horizontal flow, and it can support strong vertical motion. Upwelling at a current discontinuity caused by a sudden change of bottom slope has been predicted by Johnson and Killworth (1975) and Killworth (1973). For the upwelling to reach the surface, a horizontal divergence mechanism is needed to satisfy mass continuity. In coastal upwelling, this is provided by the wind-driven offshore Ekman flow. In the case of a front, a current discontinuity can be created by the discontinuity of density at the surface (Csanady 1971), and the upwelling can be forced by an interfacial Ekman flow induced by the vertical shear at the bottom of the frontal layer, as illustrated in Fig. 19. The possibility of upwelling by this mechanism has been demonstrated by Tang (1982) using a thin slab to model the frontal layer. His results show a circulation pattern basically of the form shown in Fig. 18. The numerical model of James (1978) also indicates a cross-front circulation of this type.

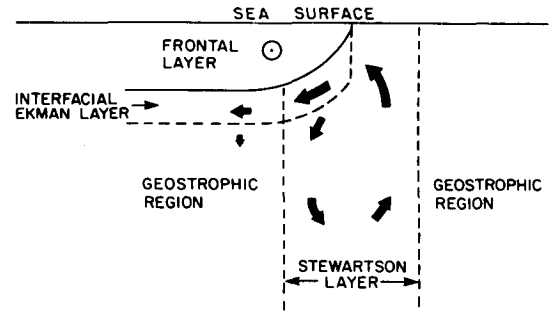

FIG. 19. Schematic diagram to illustrate the generation mechanism of the cross-front flow. The vertical shear layer may consist of several sublayers. Here only the thickest layer, the Stewartson layer, is shown. Details of the layer structure are given in Tang (1982).

10. Summary and conclusions

- The frontal system is formed by the injection of buoyancy into a semi-enclosed area. The light water at the mouth of the estuary creates a horizontal density gradient which drives a counterclockwise geostrophic flow carrying the estuarine water downstream along the coast forming the coastal jet Gaspé Current.
- Across the frontal zone, there are three distinct regimes of differing T–S characteristics: (a) inside the front; (b) from the tip of the frontal layer extending to a distance of 25 km (for the cross-channel front) or 10 km (for the front along the Gaspé Coast); and (c) outside of regime (b). In regime (c) the T–S relationship indicates vertical mixings of three water types. In regime (b), the water has the same T–S characteristics as in regime (c), but the vertical distributions of T–S are quite different. In particular, the surface temperature in regime (b) is lower than that in regime (c) by 2.5°C. The frontal layer itself is composed entirely of the estuarine water and is separated from the ambient water by a sharp interface.
- The distributions of the water masses were studied by calculating the percentage contents of the various water types. The results show that the water with a given T–S value is at shallower depths in regime (b) than in regime (a).
- The cross-front momentum balance is mainly geostrophic.
- The thickness of the surface mixed layer varies across the front. In regime (c), the mixed layer is well developed with a sharp boundary at 20 to 25 m. The thickness drastically decreases in regime (b) and in several stations the mixed layer disappears altogether. Near and within the frontal layer, the mixed layer is reestablished but with a reduced thickness.
- Horizontal intrusions of water masses occur in two regions: underneath the frontal layer, and in the intermediate cold layer. The origin of the intruding water underneath the frontal layer is the Gulf surface

water. In the intermediate cold layer, interleaving of thin layers of thickness of about 5 m was observed in localized regions.

- A cross-front circulation is proposed to explain the observations.
- Two mechanisms for the cross-front flow and frontal upwelling are discussed. One is the vertical motion forced by the centripetal acceleration of the water parcels flowing along a curved isopycnal. The second is the suction of the subsurface water outside the front by an internal Ekman flow beneath the frontal layer induced by the strong shear across the frontal boundary.

A consequence of the frontal upwelling is a downward heat flux and an upward salt and nutrient flux. Indeed, Bugden (1981), using historical data to calculate the salt and heat budgets of the GSL, found that most of the vertical volume, heat and salt transports take place in the northwestern GSL and nutrient fluxes implied by the calculated upwelling are capable of supporting the estimated primary production.

In conclusion, we emphasize that the frontal dynamics and characteristics are dependent on the type of the front and its generation mechanism. What we observed in the GSL may be found in other frontal systems only if a similar oceanographic environment exists. Two possible candidates are the fronts formed by lighter Atlantic surface water entering the Mediterranean through the Strait of Gibraltar (Wanamaker, 1979) and the front formed by the warm water of the Japan Sea flowing into the Pacific through the Tsugaru Strait (Hata 1973).

Acknowledgments. I wish to thank J. D. Woods, E. P. W. Horne, B. D. Petrie, J. W. Loder and P. C. Smith for discussions that helped to clarify many points in the paper, and Dequan Yang for assistance in the preparation of the manuscript.

REFERENCES

Benoit, J., 1980: Variation temporelles et spatiales du Courant de Gaspé. M.Sc. thesis, Université du Québec à Rimouski, 53–54.

Bowman, M. J., 1977: *Oceanic Fronts in Coastal Processes.* M. J. Bowman and W. E. Esaias, Eds., Springer-Verlag, 6–13.

Bugden, G. L., 1981: Salt and heat budgets for the Gulf of St. Lawrence. *Can. J. Fish. Aqua. Sci.*, **9**, 1153–1167.

Coachman, L. K., and R. L. Charnell, 1979: On lateral water mass interaction—a case study, Bristol Bay, Alaska. *J. Phys. Oceanogr.*, **9**, 278–297.

Csanady, G. T., 1971: On the equilibrium shape of the thermocline in a shore zone. *J. Phys. Oceanogr.*, **1**, 263–270.

El-Sabh, M. I., 1976: Surface circulation pattern in the Gulf of St. Lawrence. *J. Fish. Res. Board Can.*, **33**, 124–138.

Forrester, W. D., 1964: A quantitative temperature-salinity study of the Gulf of St. Lawrence. Bedford Inst. Rep. 64–11, 9.

Garrett, C., 1979: Mixing in the ocean interior. *Dyn. Atmos. Oceans*, **3**, 239–265.

Garvine, R. W., 1980: The circulation dynamics and thermodynamics of upper ocean density front, *J. Phys. Oceanogr.*, **10**, 2058–2081.

Hata, K., 1973: Variations in hydrographic conditions in the seas adjacent to the Tsugaru Straits. *J. Meteor. Res.*, **25**, 467–479.

Horne, E. P. W., 1978: Interleaving at the subsurface front in the slope water off Nova Scotia. *J. Geophys. Res.*, **83**, 3659–3671.

Hoskin, B. J., and F. P. Bretherton, 1972: Atmospheric frontogenesis models: mathematical formulation and solution. *J. Atmos. Sci.*, **29**, 11–37.

Ingram, R. G., 1979: Water mass modification in the St. Lawrence Estuary. *Nat. Can.*, **106**, 45–54.

James, I. D., 1978: A note on the circulation induced by a shallow-sea front. *Estuarine Coastal Mar. Sci.*, **9**, 197–202.

Johnson, J. A., and P. D. Killworth, 1975: A bottom current along the shelf break. *J. Phys. Oceanogr.*, **5**, 185–188.

Joyce, T. M., 1977: A note on the lateral mixing of water masses. *J. Phys. Oceanogr.*, **7**, 626–629.

——, W. Zenk and J. M. Toole, 1978: The anatomy of the Antarctic polar front in the Drake Passage. *J. Geophys. Res.*, **83**, 6093–6113.

Kao, T. W., 1980: The dynamics of oceanic fronts. Part I: The Gulf Stream. *J. Phys. Oceanogr.*, **10**, 483–492.

Killworth, P. D., 1973: A two-dimensional model for the formation of Antarctic Bottom Water. *Deep-Sea Res.*, **20**, 941–971.

MacVean, M. K., and J. D. Woods, 1980: Redistribution of scalars during upper ocean frontogenesis: A numerical model. *Quart. J. Roy. Meteor. Soc.*, **106**, 293–311.

Mooers, C. N. K., 1978: Oceanic fronts: A summary of a Chapman Conference. *Trans. Amer. Geophys. Union*, **5**, 484–487.

——, C. A. Collins and R. L. Smith, 1976: The dynamic structure of the frontal zone in the coastal upwelling region off Oregon. *J. Phys. Oceanogr.*, **6**, 3–21.

Needler, G. T., 1978: Discussionists' comments on "High latitude processes for ocean climate modelling." *Dyn. Atmos. Oceans*, **3**, 231–237.

Pingree, R. D., and D. K. Griffiths, 1980: A numerical model of the M_2 tide in the Gulf of St. Lawrence. *Oceanol. Acta*, **3**, 221–225.

Ruddick, B. R., and J. S. Turner, 1979: The vertical scale of double-diffusive intrusions. *Deep-Sea Res.*, **26A**, 903–913.

Tang, C. L., 1980a: Mixing and circulation in the northwestern Gulf of St. Lawrence: A study of a buoyancy-driven current system. *J. Geophys. Res.*, **85**, 2787–2796.

——, 1980b: Observation of wavelike motion of the Gaspé Current. *J. Phys. Oceanogr.*, **10**, 853–860.

——, 1982: A model for frontal upwelling. *Hydrodynamics of Semienclosed Seas*, J. Nihoul, Ed., Elsevier, 329–348.

——, and A. S. Bennett, 1981: Physical oceanographic observations in the northwestern Gulf of St. Lawrence, 1978–1980. Bedford Inst. Data Series, BI-D-81-6, 23–77, 117–120.

Wanamaker, B., 1979: The Alboran Sea gyre: ship, satellite and historical data. SACLANTCEN Rep. SR-30, 1–5.

Woods, J. D., R. L. Wiley and M. G. Briscoe, 1977: Vertical circulation at fronts in the upper ocean. *A Voyage of Discovery*, M. Angel, Ed., *Deep-Sea Res.*, **24** (Suppl.) 253–275.